



**HAL**  
open science

# Landslide tsunami vulnerability in the Ligurian Sea: case study of the 1979 October 16 Nice international airport submarine landslide and of identified geological mass failures

M. Ioualalen, S. Migeon, O. Sardou

► **To cite this version:**

M. Ioualalen, S. Migeon, O. Sardou. Landslide tsunami vulnerability in the Ligurian Sea: case study of the 1979 October 16 Nice international airport submarine landslide and of identified geological mass failures. *Geophysical Journal International*, 2010, 181 (2), pp.724 - 740. 10.1111/j.1365-246X.2010.04572.x . hal-00468916

**HAL Id: hal-00468916**

**<https://hal.science/hal-00468916>**

Submitted on 2 Oct 2021

**HAL** is a multi-disciplinary open access archive for the deposit and dissemination of scientific research documents, whether they are published or not. The documents may come from teaching and research institutions in France or abroad, or from public or private research centers.

L'archive ouverte pluridisciplinaire **HAL**, est destinée au dépôt et à la diffusion de documents scientifiques de niveau recherche, publiés ou non, émanant des établissements d'enseignement et de recherche français ou étrangers, des laboratoires publics ou privés.



Distributed under a Creative Commons Attribution 4.0 International License

# Landslide tsunami vulnerability in the Ligurian Sea: case study of the 1979 October 16 Nice international airport submarine landslide and of identified geological mass failures

M. Ioualalen,<sup>1</sup> S. Migeon<sup>1</sup> and O. Sardoux<sup>2</sup>

<sup>1</sup>*GéoAzur, IRD - CNRS - OCA - UNSA, Villefranche-sur-mer, France. E-mail: Mansour.Ioualalen@geoazur.obs-vlfr.fr*

<sup>2</sup>*GIS-CURARE, Valbonne, France*

Accepted 2010 February 19. Received 2010 January 13; in original form 2009 February 24

## SUMMARY

The Ligurian sea, at the France–Italy boarder of the Mediterranean Sea, has experienced in the past numerous submarine landslides within its very near continental slope, the continental shelf being very narrow. The most recent occurred on the 1979 October 16 near Nice international airport and generated tsunami waves of order 3 m of amplitude in some specific locations. More ancient landslides are also easily identified through bathymetric surveys of the seafloor. For the 1979 event we propose two distinct tsunamigenic landslides based on identified scars observable on the seafloor. The first one corresponds to the volume Vol1 that slid at the airport (in shallow water) while the second one corresponds to the more substantial volume Vol2 that has been localized at the slope. Former studies indicate that only the combination of the two slides may explain the event. We complement these studies by asserting that when the two slides are taken separately, they already explain a significant (although not a total) part of the event: Vol1 explains partly the tsunami observations in the vicinity of the airport while Vol2 contributes to explain the ones away from the area, in particular at Antibes where the highest wave has been observed. The modelling effort is then extended to evaluate the tsunamigenesis of selected (but representative) former landslides having a clear scar signature. The vulnerability of the area to landslide-triggered tsunami is then proposed to discussion along with possible mechanisms that can be responsible for local wave amplification.

**Key words:** Numerical solutions; Tsunamis; Submarine landslides; Europe.

## 1 INTRODUCTION

Tsunamis are typically related to several triggering factors including earthquakes generated along rupture zones extending several tens to hundreds kilometres long, the gravitational massive collapse of volcano edifices or coastal cliffs, and submarine landslides (Tinti *et al.* 1999; Fryer *et al.* 2004; McAdoo & Watts 2004). Until recent years, failure-induced tsunamis were generally thought to be rare, much localized and of lower energy than seismically generated tsunamis. Recent studies revealed that failure-induced tsunamis could be at least as frequent as the earthquake-induced ones and could also produce destructive coastal waves (McMurthy *et al.* 2004; Lee *et al.* 2007). In the present-day demographical and industrial expansion of the coastline areas all over the world, these are important results implying that tsunami hazard and assessments must not only be studied in tectonically active areas but also in more tectonically passive contexts where submarine failures can be very common through time (Garziglia *et al.* 2007).

The Ligurian sea, offshore the coastal area between the cities of Cannes (the French Riviera) and Bordighera (Italy) has experienced

in the past numerous tsunamis (Pelinovsky *et al.* 2001) as well as Submarine Mass Failures (SMFs). The presence of SMFs is evidenced by consequent scars still visible on the present-day seafloor (Fig. 1). The wide diversity of the scars characteristics (their slope, volume, location, depth) necessarily raises the question on their tsunami-triggering potential. It is of crucial interest to study if some of them could have had a tsunamigenic potential as 2 million people are now living along the coastline between the cities of Nice and Genoa and some failure events could potentially still trigger at any places along the continental slope. If so, at which extent in terms of coastal vulnerability, and then, how would be the waves guided in the area? and what should be their mode of amplification? Return period of such events are unknown obviously. However, they are sufficiently abundant to anticipate statistically further ones. In addition, recent seismic surveys have shown that the continental slope is subject to potential unstable volumes (Migeon *et al.* 2007). Their potentiality to generate tsunamis in that area has been already set up since the 1979 October 16 tsunami that has been generated by a landslide in the immediate vicinity of Nice international Airport. If the cause of the tsunami is clear as it has been established that

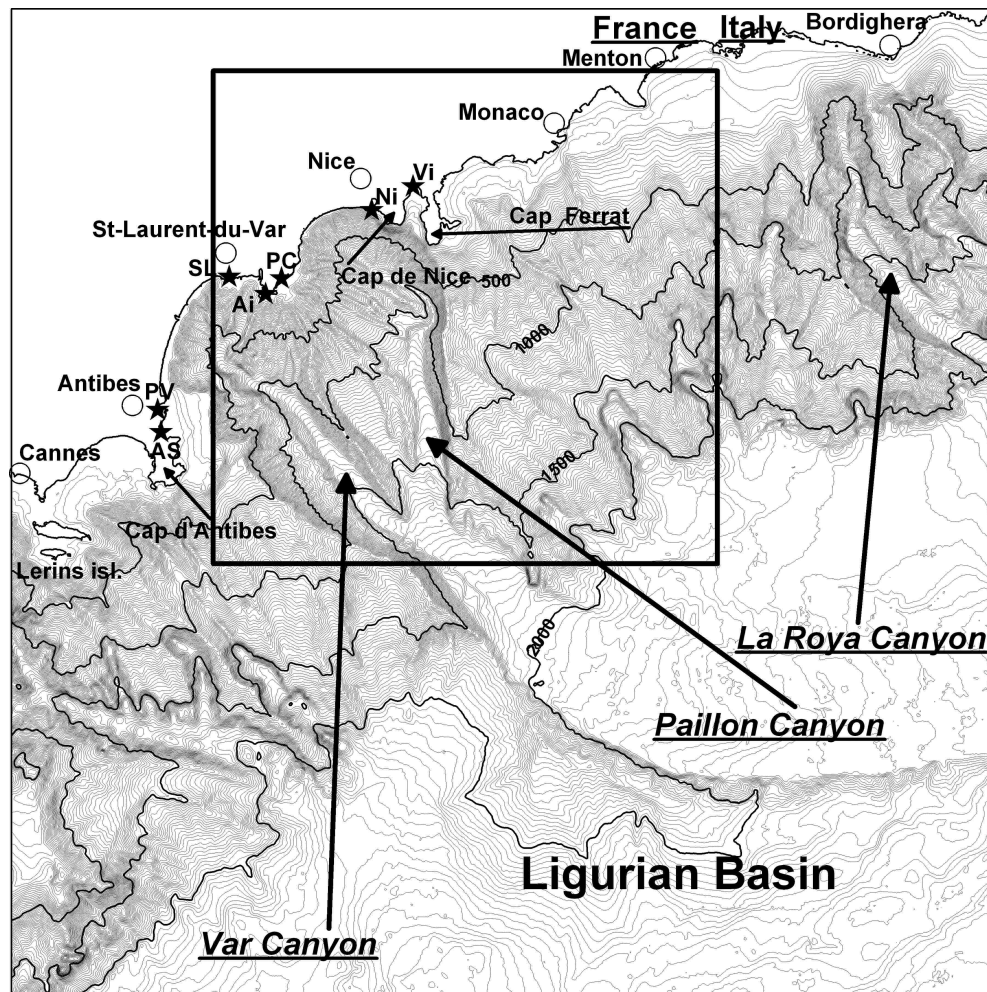


**Figure 1.** Ligurian coast and sea. The geographical area represents the computational domain. Bathymetry is plotted with 20 m iso-contours (500 m iso-contours in bold). Stars represent locations mentioned in the text (taken from Assier-Rzadkiewicz *et al.* 2000): Vi for Villefranche-sur-mer, Ni for Nice harbour, PC for Port de Clapage, Ai for Nice international airport, SL for Saint-Laurent du Var, PV for Port Vauban in Antibes, and AS for Antibes-La-Salis beach. The virtual tide gauges are located at the nearest grid point from the coastline (100 m away) and range from 2 to 6 m depth depending on the local slope.

no earthquake was recorded in the area, the actual conditions of the 1979 landslide(s) are still unclear and several studies have tried to explain the mode of triggering of the slide (Piper & Savoye 1993; Habib 1994; Mulder *et al.* 1997; Assier-Rzadkiewicz *et al.* 2000; Dan *et al.* 2007). The slide together with the propagating tsunami have been computed by Assier-Rzadkiewicz *et al.* (2000), but their study does not totally reproduce the available observations. This is the reason why we try other slightly different scenarii in the present paper and we perform a closer analysis of the simulated sequence of event.

For the purpose of studying failure-induced tsunami in the Ligurian Sea we first perform a reference simulation based on the 1979 October 16 landslide(s). Further scenarii of the event are tested. Like Assier-Rzadkiewicz *et al.* (2000) we have introduced two SMFs that have been simulated distinctly to evaluate their respective contribution to the observed tsunami. In particular are their respective contributions sufficient to explain the event at different locations or is it more complex? Then, based on the methodology, we study if older geological SMFs that have been identified on the slope could have been tsunamigenic and at which extent. A generic vulnerability map is ultimately provided with a tentative explanation of the local modes of wave amplification yielding the variation of the coastal vulnerability of the area.

## 2 GEOLOGICAL SETTING

### 2.1 The 1979 Nice tsunami observations and previous simulations

Abundant scientific papers and expert reports deal with the so-called 1979 event that is probably one of the most media geological event that happened in France within the last 20 yr. In addition to the scientific analysis of the event, valuable observations mainly coming from eyewitnesses and gathered and reported by Assier-Rzadkiewicz *et al.* (2000) are used in the following section to depict the whole sequence of events.

On 1979 October 16, at 13:57 hr local time, a failure occurred at shallow water depth during infilling operations related to the construction of the new Nice harbour. The failure affected both underconsolidated silty-clayey deposits of the upper continental slope and some of the landfill aggregates. This event was very sudden and the extension of the airport slid in to the sea within a time interval of few minutes. At the same time, witnesses located onshore observed a sea-level fall of tens of metres and about eight minutes later, three successive waves broke along the coastline between Nice and Antibes. As no earthquake was recorded at the time of the failure and tsunami, the tsunami must be related to SMF(s).

The event caused the death of nine people taken away on top of the sliding masses at the airport and another one happened to be 10 km away, in the Antibes city, where a beach has been inundated. The causes of the triggering of the landslide are still much debated (Dan *et al.* 2007) but that point is not the purpose of the paper.

There is no evidence that the tsunami has been directly generated by the shallow-water landslide itself or by a possible subsequent deeper one. There is no objective data like tide gauge records to reconstruct in details the relationship between the failure and the tsunami because those of Nice and Villefranche-sur-mer cities have a sampling frequency lower than the tsunami itself. The available information about the tsunami are only based on eyewitnesses who have always to be considered carefully in the case of an unusual catastrophic geological event. As an example, even a low-amplitude tsunami wave may be somewhat destructive and witnesses will then unconsciously amplify it. The information gathered in the MIP (1981) report and analysed by Assier-Rzadkiewicz *et al.* (2000) refer mainly to the amplitude, the wave period and the chronology of the event. They are mentioned again here strictly as Assier-Rzadkiewicz *et al.* (2000) did, time  $t_0$  being the occurrence of the airport landslide (13h57).

Between  $t_0$  and  $t_0 + 1$  min (13h58), wave oscillations are observed at Saint-Laurent du Var (SL): all following abbreviations in the text refer to geographic locations on Fig. 1. Their period is  $\sim 3$  min. The leading edge is a trough larger than 2 m amplitude, then crests and troughs weaker than 1 m amplitude follow until 14:50 hr.

At  $t_0 + 5$  min (14h02), oscillations of period larger than 7 min led by a crest are observed at the Port de Clapage (PC), located at  $\sim 1$  km east of Nice international Airport (AI). The first crest is as high as 2–3 m 8 min-period oscillations with an  $\sim 1.2$  m amplitude and led by a crest are witnessed at Nice Harbour (Ni).

At  $t_0 + 9$  min (14:06 hr), three oscillations of equal amplitude (2.5–3.5 m) and of period of  $\sim 9$  min led by a crest are observed at Antibes-La-Salis beach (AS). At this location, oscillations ended at 14:30 hr. Similar oscillations are observed at the Port Vauban in Antibes (PV) with a 1 min lag and of lower amplitude.

At  $t_0 + 11$  min (14:08 hr), 8 min-period oscillations led by a crest were observed at Villefranche-sur-mer harbour (Vi). The first crest amplitude is estimated to be of 1.8 m in height.

Special modelling efforts have been already dedicated to this event for two main reasons: (i) the event caused nine casualties and (ii) since the SMF occurred during the extension of the nearby PC harbour works it is crucial to determine the possible anthropic responsibilities. With a simple ray theory the MIP (1981) report study found some accurate tsunami arrival times but encountered a lack of coherence on the sequence of events. In particular, oscillations at SL, appeared too early. Besides, the wave amplitude, even recalibrated, was far from being coherent at AS. Habib (1994) simulated a sediment debris flow with a time lag to reproduce the arrival time at SL. The most comprehensive simulation has been performed by Assier-Rzadkiewicz *et al.* (2000). The authors simulated the slide and the tsunami propagation with non-linear shallow water models. The fact that fairly eye witness reports indicated two wave periodicities ( $\sim 3$  and 8–9 min) motivated Assier-Rzadkiewicz *et al.* (2000) to propose a scenario taking into account two slides. The first slide (shallower one) took into account the collapse of a part of the airport and the second, more voluminous and potentially triggered at greater water depth, was likely to explain the steep wave at AS. However, the scenario and their carefully run simulations did not reproduce the whole set of observations. In particular, contrary to observations, a trough leads their simulated tsunami at AS location and simulated periods were quite different from the reported

ones. Besides, the amplitudes are relatively coherent, although they appear to be overpredicted. Regards to this latter issue, a sensitivity test on the frequency dispersion effects will be performed here in order to check if the lack of dispersion in their model (taken into account in the present simulations) is responsible for these over-predictions and for the lack of coherent periods representation. We propose here to use more coherent SMFs volumes and locations and a different numerical model: a fully non-linear Boussinesq model FUNWAVE compared to their Shallow water model.

## 2.2 Slope morphology, sediment supply, and submarine landslides offshore the Nice-Monaco coastline

The French Ligurian margin is characterized by a narrow continental shelf (1–2 km) that could be even less than 200-m wide at specific location like along the ‘Baie des Anges’, in front of the Nice city and airport. The slope break is thus located very close to the coastline, at 50–100 m of water depth as an average, but could be much shallower. Then, a steep continental slope extends over 20 km to a water depth of 2000 m with an average angle of  $11^\circ$  (Cochoat *et al.* 1993). In that area, the slope is eroded by three main underwater canyons that connect directly to the Var, the Paillon and the La Roya rivers (Fig. 1). They are small mountain-supplied rivers that experience violent flash floods every year, during fall and spring times, as a result of snow melt and convective rainfall. The average water discharge of the Var river, about  $50 \text{ m}^3 \text{ s}^{-1}$ , can increase 10-fold during floods, and suspended sediment concentration can reach tens of  $\text{kg m}^{-3}$ . The Var river carries yearly approximately  $1.5 \times 10^6$  tons of particles that might generate a 63 mm to 54 cm yearly sedimentation rate on the upper slope around the river mouth (Mulder *et al.* 1996). As a result, the sedimentary deposits accumulating from the top to the base of the continental slope builds up unstable underconsolidated areas that are likely to slide (Klaucke *et al.* 2000). Evidences of failure events have been reported from multibeam, seismic-reflection and sidescan sonar data (Klaucke & Cochoat 1999; Migeon *et al.* 2007). Offshore the Nice city (France), mass-wasting events mainly affect the upper part of the slope, in areas close to the Var and Paillon river mouths, where volume of fresh sediment delivered by rivers is the highest. Small-scale failures ( $\leq 100$  m wide) are mainly located near the shelf break; they are the most abundant type of failures and are restricted to the uppermost layers (up to 10 m) of slope sediment (Migeon *et al.* 2007). Larger-scale failures (up to 400 m wide) are located deeper on the slope and they affect deposits over greater thickness (up to 40–50 m). Eastward, offshore the Beaulieu-Menton area, impressive scars like the so-called Cirque Marcel are located near the base of the slope, between 1300 and 2000 m of water depth and affect slope deposits over 100–300 m.

## 3 THE NUMERICAL PROCEDURE AND THE COMPUTATIONAL DOMAIN

The computation of a SMF-derived tsunami first requires the calculation of the water-column deformation due to the SMF slide. This is generally done by running a numerical model based on potential flow assumptions. Here, we refer to the work of Grilli *et al.* (2002) who developed a boundary element method (BEM). In order to avoid a systematic full calculation of the tsunami generation stage, Grilli *et al.* (2002) proposed a procedure that estimates the tsunami initial condition at low coast in terms of CPU. The first step is to identify the movement of the deformable body (the SMF) to the one of its centre of mass: Watts & Grilli (2003) showed that the deformation of

SMF contributes at second order only to the tsunami generation as far as the SMF slide is relatively fast. As a result, SMF slide features like the initial acceleration, the terminal velocity, and characteristic time and distance are derived from the centre of mass movement (Watts 1998; Grilli *et al.* 2002). Then, once the numerical simulations have been validated with experiments of Watts (1998), they performed a representative ensemble of numerical experiments and they derived empirical functions that provide the free surface elevation of any SMF depending on its shape (density, volume and slide orientation) and on the local bathymetry (slope, depth). They considered for both experiments and numerical sliding bodies shaped like semi-ellipses. The procedure is implemented in the version 1.2 of the ‘Tsunami Open and Progressive Initial Conditions System’ (TOPICS). Besides, during the SMF-derived tsunami generation, Watts (1998) showed that almost all of the far-field wave energy is associated to potential energy. As a result, an everywhere-zero horizontal velocity field is prescribed in TOPICS. The software provides a tsunami initial condition at time, as if results from the models of Grilli *et al.* (2002) were being transferred directly to FUNWAVE tsunami propagation model at that instant of time. The package TOPICS/FUNWAVE is the widely used GEOWAVE software.

Briefly, the FUNWAVE tsunami propagation and run up model is fully non-linear and dispersive, retaining information to leading order in frequency dispersion  $O[(kh)^2]$  and to all orders in non-linearity  $a/h$  (where  $k$  denotes an inverse wavelength scale,  $a$  denotes a wave amplitude, and  $h$  denotes a water depth) (Wei & Kirby 1995; Wei *et al.* 1995). The model includes a moving

shoreline (Chen *et al.* 2000; Kennedy *et al.* 2000), bottom friction, energy dissipation to account for the wave breaking and a subgrid turbulence scheme (Wei & Kirby 1995; Chen *et al.* 2000; Kennedy *et al.* 2000).

GEOWAVE can simulate multiple tsunami sources with different generation mechanisms, occurring at different times. It has been validated based on case studies of a pyroclastic flow generated tsunami (Waythomas & Watts 2003) and several underwater landslide generated tsunamis (Watts *et al.* 2003). It has also been applied to a debris flow generated tsunami (Walder & Watts 2003). For coseismic sources it has been successfully used to simulate the 2004 December 26 Indian Ocean mega-thrust earthquake-triggered tsunami (Grilli *et al.* 2007; Ioualalen *et al.* 2007a,b) and the 1999 November 26 Vanuatu tsunami (Ioualalen *et al.* 2006).

In this study, the computational domain extends from Cannes (French Riviera) to east of Bordighera (Italy) and covers an area ranging from the coastal zone to the middle part of the Ligurian Basin (Fig. 1). The grid spacing is 100 m in both horizontal directions ( $1232 \times 1239$  nodes) and consequently the time step has been taken to 0.15 s in order to avoid numerical instabilities. One hour of propagation has been simulated. At the domain boundaries a sponge layer composed of 25 nodes has been applied (Wei & Kirby 1995; Wei *et al.* 1995). The domain has been optimized in order to obtain a reasonable description of the bays. It includes the landslide source (Fig. 2) and, most of its estimated displacement and the nearly complete tsunami initial solutions. Besides, the lateral boundaries of the

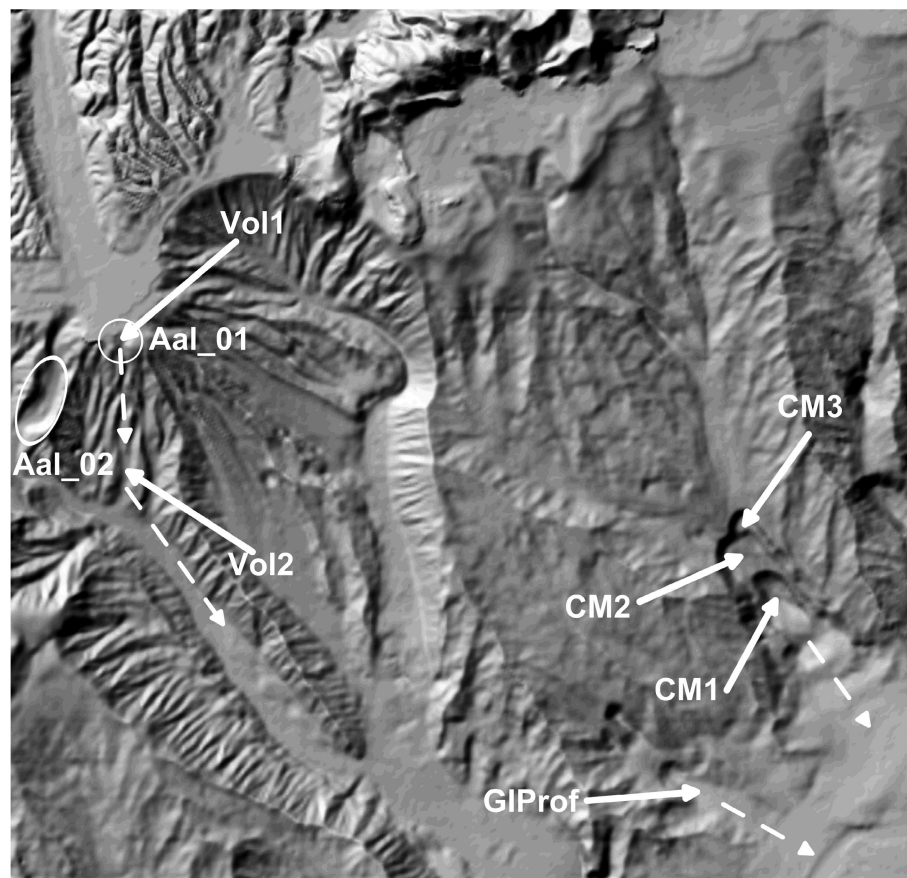


**Figure 2.** Identification of the Submarine Mass Failures (SMFs) described in Table 1 within the area represented by a rectangle in Fig. 1 along with the bathymetry mesh. The dashed lines represent their prescribed slide direction: identical for (CM1, CM2 and CM3); Ellipses are the locations of the SMFs studied by Assier-Rzadkiewicz *et al.* (2000), noted here Aal\_1 and Aal\_2.

domain have been also optimized such that no coastal reflection or bores are forgotten (Wei & Kirby 1995).

The bathymetric data used in the study have been obtained from Simrad EM300 multibeam raw data. In shallow water (less than 50 m) areas close to the coastline, 1/50 000 digitalized SHOM marine charts operated until 1987 from Antibes to Menton have been used. The onland topography was derived from a 50 m horizontal grid-resolution product built by the Institut Géographique National (IGN).

#### 4 DESCRIPTION AND VOLUME ESTIMATION OF SELECTED LANDSLIDES

Several landslides have been selected either because they were subjected to a high level of knowledge (case of the 1979 event), or on the basis of their impressive size that was thought to potentially trigger a tsunami. Their morphology has been studied using multibeam bathymetry collected using a Simrad EM300 aboard the O/V Le Suroit (Ifremer-Genavir). Volumes of reworked deposits have been estimated using a DTM with a spatial resolution of 25 m. As the headwall scars were always well defined on bathymetric data, the Caribes and GMT softwares allowed to calculate the volume of sediment missing in the scar areas by firstly reconstructing a pre-slide seafloor topography and then subtracting the pre- and post-slid topographies.

##### 4.1 Case study of the 1979 event

The initial scar and pathway of the 1979 failure is still clearly visible on the present-day seafloor (Fig. 3). The scar lies at a water depth of 20 m, directly at the shelfbreak. It exhibits a complex morphology consisting in several coupled amphitheatre-like morphologies

(Fig. 3). Then, the scar is continuing on the slope by a thalweg that evidences the erosive power of the failed mass remobilized in the scar. The thalweg is oriented in the direction of the main slope angle and reached the Var Canyon at the water depth of 1080 m. The thalweg made two sharp bends between 400 and 550 m of water depth (Fig. 3). Its width and depth are almost constant (250 and 50 m, respectively) during the first half of the pathway (up to the second bend, representing a distance of 2.3 km from the source area). After the second bend, its width and depth increase rapidly to 600 and 60 m, respectively, suggesting a huge and rapid increase of the erosional process at the bed and the rapid incorporation of sediment resulting in an increasing volume. From the estimated velocity of the slurry flow made by Mulder *et al.* (1996), that huge and rapid increase of volume of the moving slurry probably occurred few minutes after the landslide was triggered. The whole pathway of the 1979 event exhibits a quasi-linear bathymetric profile (Fig. 3) and a constant slope angle of  $10^\circ$ .

From these morphological considerations, we divided the 1979 event into two main phases: the initial rupture at the shelfbreak characterized by a volume Vol1, and the later phase of erosion and increasing volume called Vol2 at a greater depth (800 m as an average). Comparison of Vol1 and Vol2 revealed that the moving slurry flow increased its volume 25 times in less than 3–4 km and in a short time period. As the TOPICS model cannot manage a gradual change of properties and volume of the moving failure, we used these two phases and their own volume to simulate the 1979 event. As the main increase of volume seems to occur after the second bend with Vol2, we did not consider any significant change of volume between Vol1 and Vol2.

Assier-Rzadkiewicz *et al.* (2000) have taken an initial volume of  $8.7 \times 10^6 \text{ m}^3$  for Aal\_1, their equivalent SMF of our Vol1 (Fig. 2). They reconstructed the slid volume by subtracting a bathymetric map generated before the landslide and one generated about

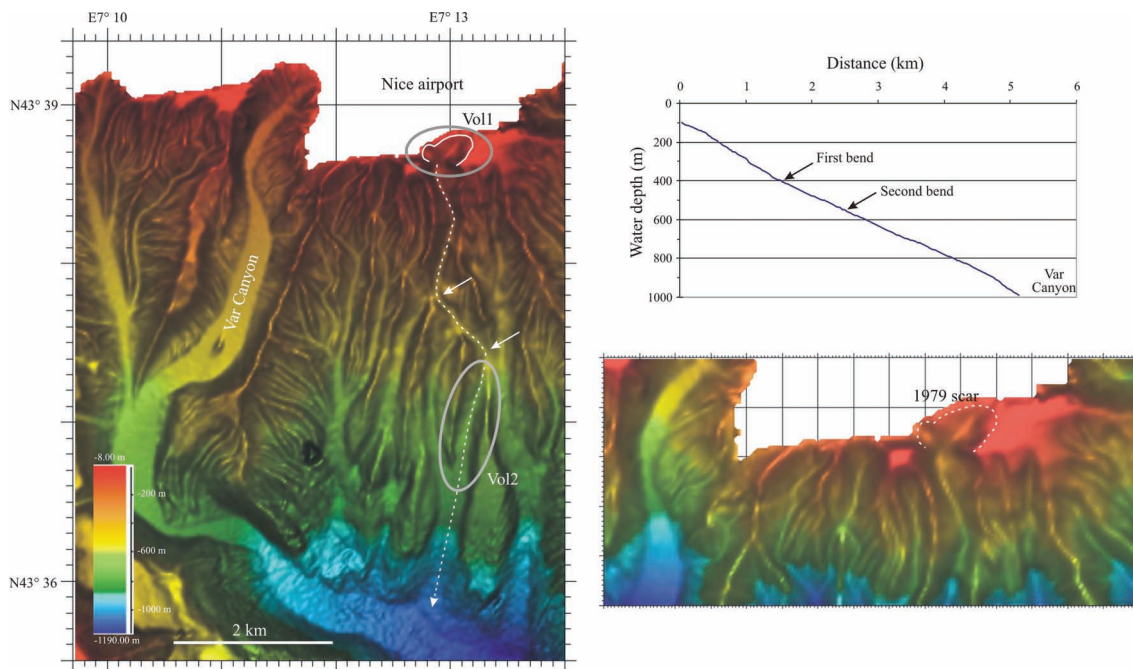


**Figure 3.** Bathymetric maps showing the morphology of the continental slope offshore the Nice airport, the location of the scar of the 1979 event and the pathway of the reworked deposits on the slope (white dashed line). The location of Vol1 and Vol2 discussed in the text are also represented. The bathymetric profile is taken along the pathway of the 1979 event, from the base of the scar to the Var Canyon. The two arrows locate the two bends observed along the pathway of the 1979 event.

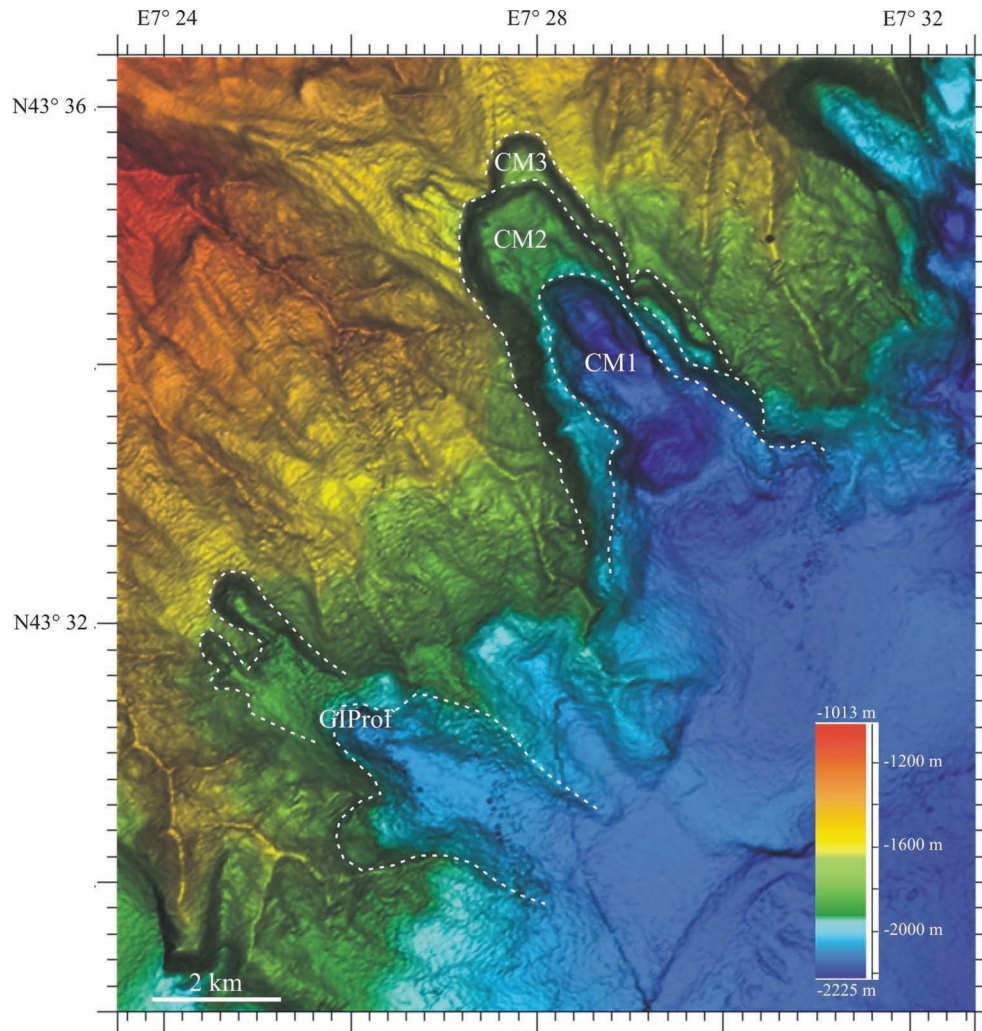


**Figure 4.** Bathymetric map showing the morphology of huge submarine landslides triggered at the base of the continental slope. The white dashed lines are the limits of the calculated volumes CM1, CM2, CM3 (CM is for Cirque Marcel) and GIProf (see text for explanation).

**Table 1.** TOPICS input data are: estimate of the volume  $V$  of each identified Submarine Mass Failure (SMF).

SMF	CM1	CM2	CM3	GIProf	Vol1	Vol2
$V$ (km <sup>3</sup> )	2.42	0.504	0.0293	0.289	0.00219	0.0622
$x_o$ (°)	7.4930°E	7.4833°E	7.4638°E	7.4496°E	7.2162°E	7.2171°E
$y_o$ (°)	43.5542°N	43.5822°N	43.5918°N	43.5130°N	43.6454°N	43.6071°N
$d$ (m)	2095	1788	1708	2052	47	814
$L$ (m)	5724	1838	959	3553	652	3027
$l$ (m)	2849	1684	741	1850	346	458
$w$ (m)	148	163	41	44	10	45
$\phi$ (°)	216	216	214	241	182	216
$\theta$ (°)	4	4	4	4	12	10
$\lambda_c$ (m)	50753	26570	18758	39574	1082	14582
$a_i$ (ms <sup>-2</sup> )	0.20	0.20	0.20	0.20	0.61	0.51
$v_t$ (ms <sup>-1</sup> )	72	41	30	57	31	83
$t_c$ (s)	354	200	145	279	50	163
$d_c$ (m)	25700	8239	4299	15926	1551	5886
$C_i$ (m)	0.26	0.15	0.018	0.032	1.38	0.20
$T_i$ (m)	-0.66	-0.16	-0.013	-0.078	-4.81	-0.58

*Notes:* The longitude and latitude of the SMF centroid ( $x_o$ ,  $y_o$ ), the supposed centre of mass; The centroid initial depth  $d$  (before the slides): it corresponds to the depth of the scar center detected in the bathymetry minus half of the maximum thickness  $w$ ; The length  $L$  (Long axis) and width  $l$  (small axis) of the SMF supposed-parallaloid; The mean azimuth (direction of slide)  $\phi$  defined counter-clockwise and the mean slope  $\theta$  along slide. TOPICS output are: the characteristic initial tsunami wavelength  $\lambda_c$ , the slide initial acceleration  $a_i$ , terminal velocity  $v_t$  and its characteristic duration  $t_c$  (the wave period relative to the wave celerity at the centroid depth) and the characteristic distance  $d_c$ .  $C_i$  and  $T_i$  represent the initial crest and trough amplitudes, respectively.

10 years after the landslide. This is a robust method, as explained by Canals *et al.* (2004) in their synthesis paper about marine landslide processes. However we find fair to note that the poor precision of (at least) the pre-landslide bathymetry might have induced a severe uncertainty in their volume estimate: the map corresponding to the pre-slide morphology was generated in the late seventies. It is a compilation of isolated depth values (1) obtained from single-beam system coupled with positioning system that was not a GPS or a DGPS but a radio-navigation system like Loran-C, or (2) calculated from seismic-reflection profiles located with similar radio-navigation systems. As it was classically done at that time, isobaths were drawn manually: there is an uncertainty about their exact location (that is the interpretation of the drawer) and there is no information about depth between two successive isobaths (separated by 10 m in that case). Assier-Rzadkiewicz *et al.* (2000) did not provide information about the horizontal resolution of that map but it should be at least of about 100 m or more. The map corresponding to the post-slide morphology was acquired using a EM12-like multi-beam system and a DGPS positioning system. Assier-Rzadkiewicz *et al.* (2000) did not provide any information about the horizontal precision of the DTM used but it should be at least of about 50 m (it is a typical value of horizontal precision for a DTM obtained using EM12 data in the late 1980s/early 1990s).

In our case, we estimated the volume Vol1 of the deposits reworked during the 1979 event by estimating the volume of missing

sediment in the 1979 scar. This is also a robust method as explained by Canals *et al.* (2004). We used a DTM with a horizontal precision of about 20 m. The DTM was generated from data collected using a EM300 multibeam system coupled with a DGPS positioning. We believe that the difference between our volume estimate and the one of Assier-Rzadkiewicz *et al.* (2000) comes from the fact that we used higher-resolution data on which it was easier to delineate the real extension of the 1979 scar and on which the real depth of the scar and inner scar was better constrained.

Bearing this issue in mind we expect different responses in terms of tsunami characteristics. In particular, we may expect lower simulated wave elevation compared to those of Assier-Rzadkiewicz *et al.* (2000) and a significantly weaker first trough. Their second volume Aal\_2 is in the same order than our Vol2 (they took  $70 \times 10^6 \text{ m}^3$ ), but they placed it too much westward (arbitrary according to the authors) by comparison with the real location of the 1979 pathway. So, their second SMF is shallower than our Vol2. The differences between the two initial motions will condition the numerical results.

#### 4.2 Case study of the Cirque Marcel

Huge scars like the so-called Cirque Marcel affected the base of the slope between 1700 and 2200 m of water depth (Figs 2 and 4). They are 2–4 km wide and 4–6 km long. The Cirque Marcel

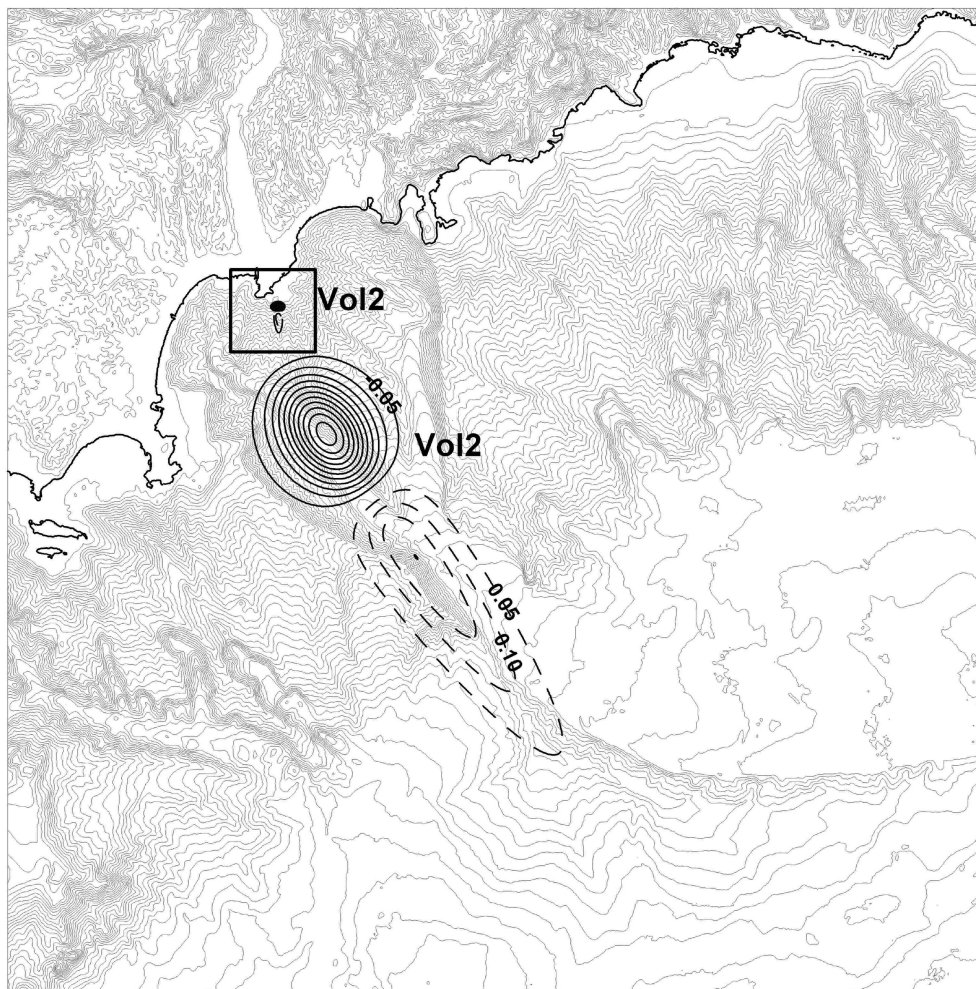


**Figure 5.** Initial surface elevation generated by TOPICS for SMFs Vol1 and Vol2. Dashed lines correspond to seafloor uplift (tsunami crest) and solid lines to subsidence (tsunami trough) (0.5 m iso-contours for Vol1 and 0.05 m iso-contours for Vol2). The bathymetry is plotted in the background (20 m iso-contours).

exhibits a complex amphitheatre-like morphology resulting from four successive scars (Figs 2 and 4). From the top to the base, the four scars have heights increasing from 100 m for the shallowest one, to 200 and 300 m and then decreasing to less than 100 m for the deepest one (Fig. 4). They are separated by flatter areas 1–2 km wide. Such failure event affected the whole Plio-Quaternary sediment pile. It is still unknown whether each scar corresponds to a single phase of sliding or if the whole Cirque Marcel corresponds to a single failure event. For sake of simplicity, we divided the Cirque Marcel into three SMFs called CM1, CM2 and CM3 (Figs 2 and 4) and considered them separately, but keeping in mind that any estimate of the derived tsunami amplitudes should be underestimated if the Cirque Marcel was in fact a single failure. In the same area, another SMF located west of the Cirque Marcel was also tested (GIProf, Fig. 2). The size of that SMF is much smaller than CM1. The characteristics of all SMFs are reported in the Table 1.

## 5 THE NUMERICAL RESULTS

In this section we discuss the numerical results for the proposed 1979 Nice airport SMF scenario. Then, based on the validity on the proposed simulated tsunami, we map the vulnerability of the area to SMFs-induced tsunamis along with the associated processes. For that purpose we simulated former tsunamis that might have been triggered by older and larger SMFs which scars are clearly identified on the bathymetric data.

### 5.1 The 1979 Nice international airport event

The computed initial waves for Vol1 and Vol2 differ significantly (Figs 5 and 6). Vol1 initial wave is approximately a decade higher amplitude than the one corresponding to Vol2 but its wavelength is approximately a decade shorter than that of Vol2 (Table 1). Besides, their mode of propagation also differs: Vol1 large axis is oriented nearly E–W while the one of Vol2 is approximately oriented NNW–SSE. As a result the main directivity of the waves are S–N for Vol1 and ENE–WSW for Vol2. Also, considering their respective wavelengths and orientations, the entire initial wave of Vol1 will be determinant for the wave impact at the coast while only the initial trough and associated following oscillations will be crucial for Vol2 (Fig. 5). Adding that there is a strong asymmetry of the initial dipole crest/trough (steeper troughs), it is likely that Vol2 will, relatively, generate a higher first wave crest (normalization made to their respective highest initial wave). Considering all these differences, it is expected that the wave impact of the tsunamis associated to Vol1 and Vol2 are far from being strictly prescribed by the maximum initial maximum load of the waves. It will be strongly related to the location of coast and to the balance between the above-cited processes at each coastal area. We may expect stronger local effects for Vol1 (near Ai, PC and SL), while, aside from this area, Vol2 tsunami will be prominent.

Time series recorded in the simulations for Vol1 indicate, as expected, strong effects locally (Ai, PC and SL; Figs 7 and 8). We obtain a leading trough everywhere but at specific points like AS

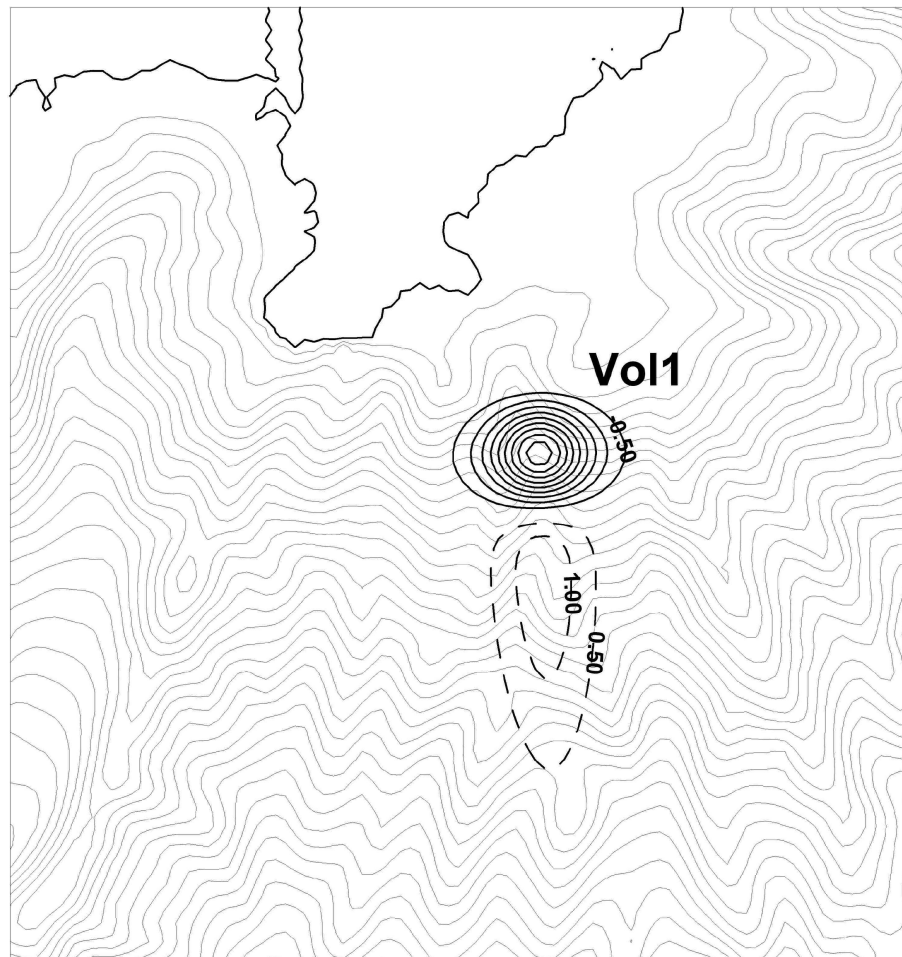


**Figure 6.** Enlargement of the area contained in the rectangle drawn in Fig. 5 (10 m bathymetry iso-contours).

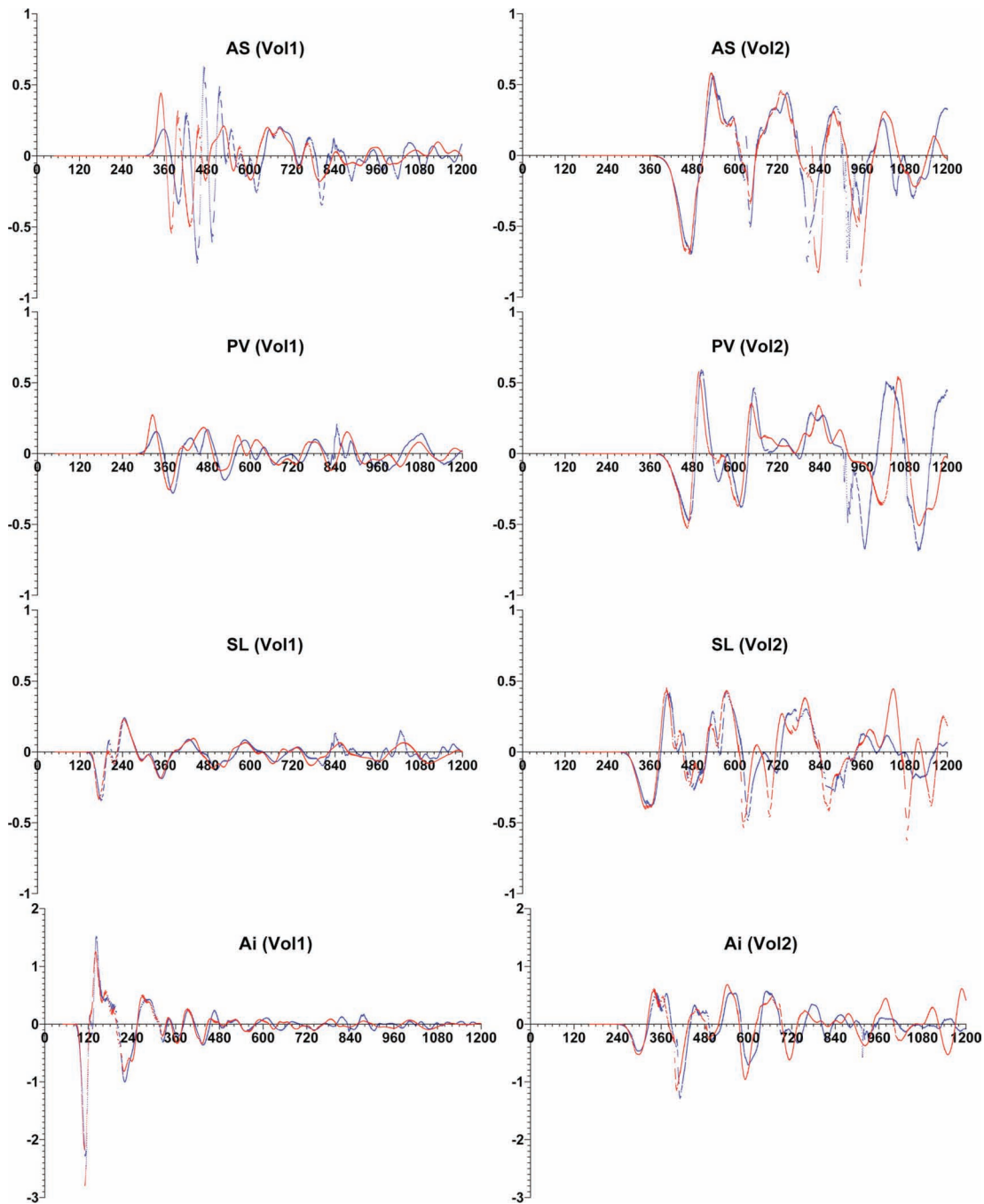


**Figure 7.** Simulated time-series (in seconds) representing the sea surface elevation (in metres) due to SMFs Vol1 and Vol2 at tide gauge locations AS, PV, SL and Ai of Fig. 1. Blue curves are for GEOWAVE Boussinesq fully non-linear model (BOUSS, dispersive) while red ones correspond to a non-linear shallow water model (NLSW, non-dispersive). Initial time  $t = 0$  corresponds to the beginning of the slide. Note that the elevation scale differs from one site to another.

and PV which are located southwest of the initial wave where the contribution of the initial trough applies first, because it propagates faster than the initial crest located at shallower water (Fig. 5). As far as the tsunami time series related to Vol2 are concerned, recorded waves at all locations are all preceded by a trough because the initial wave trough surrounds the locations area (Fig. 5). Beside the wave amplitude the main difference between tsunamis derived from Vol1 and Vol2 is the periodicity (Figs 7 and 8). It is of order of  $\sim 1$  min for Vol1 and  $\sim 3$  min for Vol2.

As far as the nature of the first wave is concerned, at AS and PV the crest/trough chronology is better reproduced by the Vol1-

derived tsunami because, contrary to Vol2 one, the wave is led by a crest as it was apparently observed (Figs 7 and 8). At this location, Assier-Rzadkiewicz *et al.* (2000) found a leading crest for their two volumes in agreement with observations. At SL, PC, Ni and Vi, both Vol1 and Vol2 tsunamis are led by troughs contrary to observations. However, at PC both simulations generate a weak first trough compared to the second. Thus, in the absence of objective observations like tide gauge records, we may propose that the second trough may have been only observed, the first crest apparently leading the wave. It is fair to say the contradiction remains. For Ni and Vi the simulations considerably underpredict the

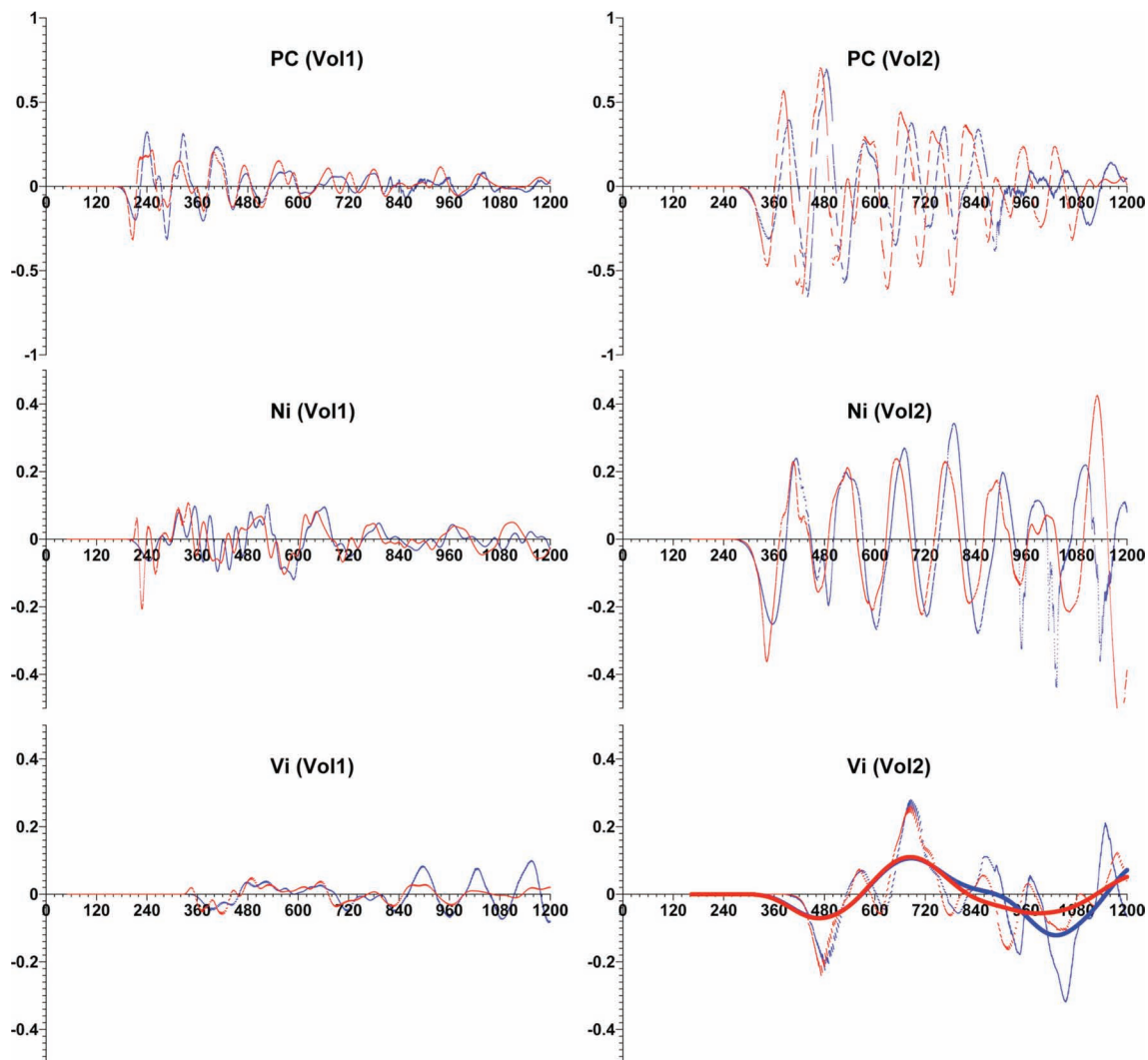


**Figure 8.** Fig. 7 continued for locations PC, Ni and Vi. A Hanning low-pass filter has been applied here for Vi–Vol2: periods lower than 5 min have been filtered: thick curves are for BOUSS (blue), NLSW (red).

observed wave amplitude and thus they do not allow any comment on the nature of the leading wave. At AS and PV, the tsunami related to vol1, simulates a leading crest as it was observed, contrary to the one related to Vol2. At SL a trough leads for Vol1 as observed and a crest leads for Vol2. Consequently, from the depression/crest chronology, Vol1 and Vol2 taken distinctly do not seem to explain directly the observed sequence of events as reported by eyewitnesses.

As far as the amplitudes are concerned west of the airport, at AS both Vol1 (1.86 m) and Vol2 (2.48 m) reasonably explain the witnessed estimation (2.5–3.5 m) with a preference to Vol2. At PV, Vol2 (1.56 m) is a better candidate (0.61 m for Vol1) (Fig. 9). At this location, Assier-Rzadkiewicz *et al.* (2000) simulated a higher wave based on their Aal\_1 volume (around 1 m) and a 4 m wave with their Aal\_2 volume. This is consistent with our results (Vol2 is the best candidate). In the vicinity of the airport, at SL, the wave amplitude generated by Vol1 (0.46 m) is closer to the witnessed estimation (less than 1 m) compared to Vol2 (2.39 m, Fig. 10). At PC, the 2–3 m wave amplitude that has been reported is better explained by the simulation using Vol1 (2.15 m) rather than Vol2 (1.75 m). To the east at Ni and Vi, both Vol1 (0.15 and 0.11 m, respectively, not shown) and Vol2 (0.62 and 0.57 m, respec-

tively, not shown) underestimate the observations (1.2 and 1.8 m, respectively).

About the arrival time at AS and PV, Vol2 is a good candidate: 9 and 8.5 min, respectively were obtained by comparison with the 9 and 8 min observed (only 6 and 6.5 min for Vol1). Close to the triggering area of SMFs, at SL, Vol1 is a good candidate (3.5 and 7 min for Vol1 and Vol2, respectively, Figs 7 and 8) compared to witnessed values, that is, between 3 and 4 min for the first crest since oscillations are observed before 1 min (a trough) with 3 min-period oscillation. At Ni, despite the underestimated wave amplitude, Vol1 is a better candidate (5 min) compared to Vol2 (7 min) and to the 5 min witnessed. The simulation at Vi is difficult to validate considering the small simulated amplitude.

To resume: it appears that Vol1 is a better candidate in terms of wave amplitude and arrival time in the airport neighbourhood (NI and SL and PC). Vol2 is relatively a better candidate than Vol1 everywhere else (away from the airport) although the amplitude are underestimated at Ni and Vi. The sequence of wave is generally not reproduced (a trough is leading in simulations while a crest has been apparently first observed with the exception of SL). Most importantly, the periodicity is not reproduced nearly everywhere (~7–9 min observed and ~2–3 min simulated). The general conclusions

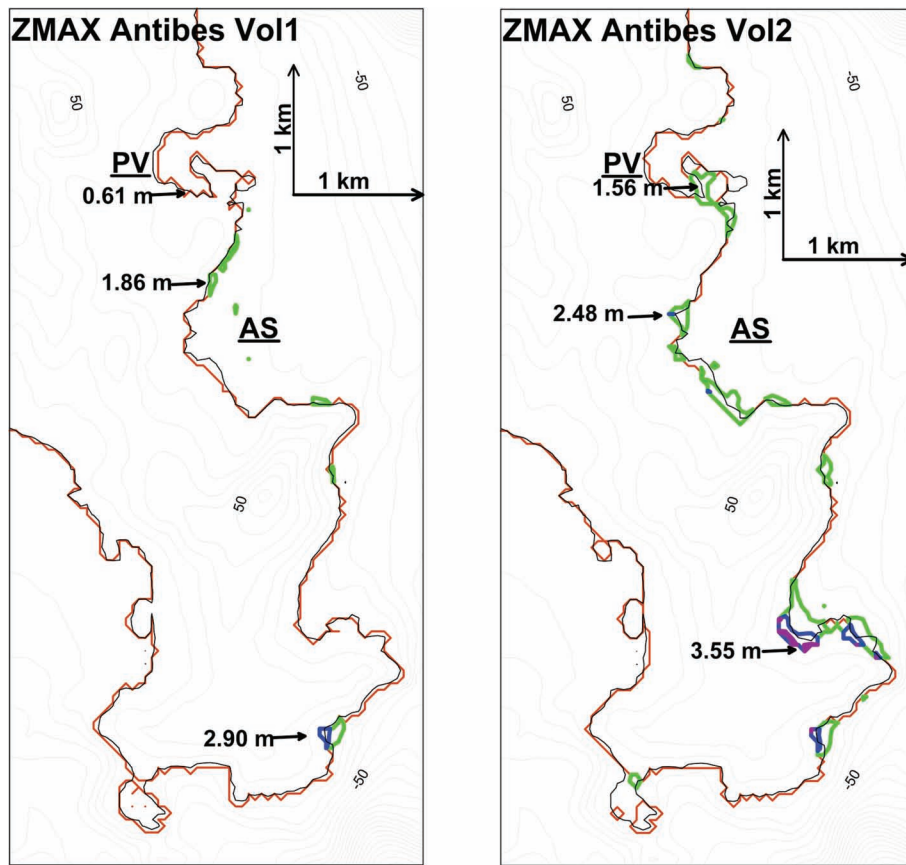


**Figure 9.** Simulated maximum of elevation for SMFs Vol1 and Vol2 at Antibes. The brown curve is for the inundation limit, coloured points are for 1 m (green), 2 m (blue) and 3 m (violet) wave elevations. The bathymetry and topography (land) are represented in the background with 10 m iso-contours. The bolded curve is for the initial coastline (before the tsunami).

are quite similar to those of Assier-Rzadkiewicz *et al.* (2000) (except at PV where their simulated the first crest), who concluded that both volumes should be considered simultaneously (and not distinctly) in order to better match the observations. We propose here a complementary interpretation by analysing the harmonic structure of the simulated tsunami waves. However, before performing such analysis we wish to insure that physical dispersion that is likely to change the spectral content of the tsunami signal is not essential here.

Since Assier-Rzadkiewicz *et al.* (2000) used a non-linear shallow water model (NLSW, non-dispersive) and we used here a non-linear Boussinesq model (NLB, dispersive), we have tested the effects of frequency dispersion. In Figs 7 and 8 we have reported the simulated tsunami waves for both models. We did not find significant discrepancies. The only usual differences concern a slight phase lag for the first crest (the group velocity differs from the phase velocity for NLB model) and a slight overprediction of the wave amplitude for the NLSW model, which is enhanced when the source is farther from the tsunami source (the dispersive effects have more time to develop). For example, for Vol2 at location Ni (close to the tsunami source) the first crest computed by the NLSW model is nearly in phase with the one computed with the NLB model while it is 10 s. in advance for Vol1 at location AS which is farther from the source. This is totally negligible regards to the tsunami arrival time discussed above. Besides, this does not change significantly the wave periodicity of the first successive crests which is another criterium used here for validation with observations. As a result the use or non-use of dispersion does not make any fair difference between

the results of Assier-Rzadkiewicz *et al.* (2000) and ours regards to the non-coherency of the wave periodicity between simulations and observations and the coherency of the arrival time.

As far as the wave amplitude for the NLSW model is concerned, we found same orders of amplitude as the Boussinesq one: (1.23, 0.26, 9.47, 1.82, 0.12 and 0.07 m) for (AS, PV, SL, PC, NI and Vi) for Vol1 and (2.51, 1.76, 2.37, 1.43, 0.60 and 0.48) for Vol2. The differences vary from  $-18$  to  $+13$  per cent for Vol2 and from  $-36$  to  $+2$  per cent for Vol1. The extreme differences for Vol1 between NLSW and NLB results are in fact matter of cms in absolute value. So the frequency dispersion does not impact the discussion above. Consequently, the overprediction of the wave amplitudes by Assier-Rzadkiewicz *et al.* (2000) cannot be attributed to the lack of dispersive effects in their simulations. Their numerical modelling itself is robust.

## 5.2 Harmonic analysis of the simulated Vol2-derived tsunami

We have computed in Fig. 11 the power spectrum of the simulated tsunami at each location for Vol2. Technically, considering the sampling (referred to the time spacing used in the simulation), we obtain more density values at high frequency than at lower frequency within a same period window. As a result the large periods are recovered more sparsely. Nevertheless, for all locations Fig. 11 evidences the  $\sim 2$ – $3$  min periods but also a significant peak around  $\sim 7$  min which is consistent with observations. In some locations like AS and Vi

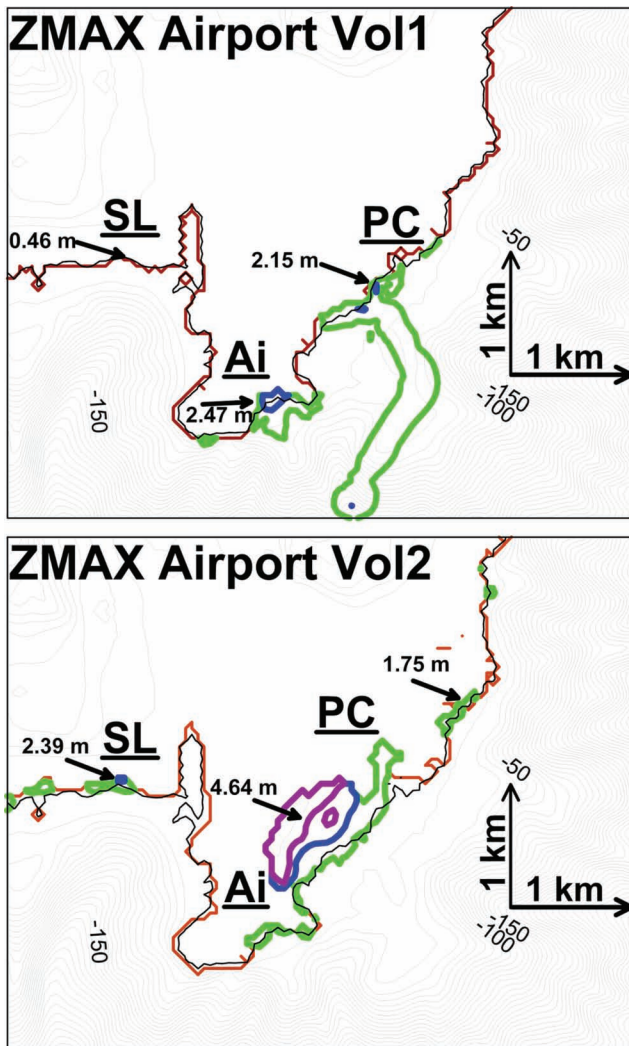


Figure 10. Same as Fig. 9 for the Airport area.

the peak is of same order of amplitude as the  $\sim 2\text{--}3$  min one. We may also conjecture that considering our sampling, actual low frequency peaks surrounding the 410 s. one (not accessible) might be higher than the 410 s. itself. There is no reason that the 410 s. is the highest low frequency peak. The figure indicates that dispersion is not crucial in the periods distribution of our case study. Besides, we have tested if non-linearity could have generated such peak. For that purpose we have performed the same simulation for a linear Boussinesq model (Fig. 11). We still obtain a nearly equivalent density distribution. The two sensitivity tests (effects of dispersion and of non-linearity) indicate that the wave spectral content has not been modified along the wave propagation. This statement is robust because we obtain relatively similar conclusions for all locations which exhibit different bathymetry shapes (open/closed bays, caps). More likely, the spectral distribution is already present in the initial wave computed with TOPICS. Although the method used in the software has to be considered with caution, it nevertheless resituates the main initial signal of the tsunami. Regards to our case study, let us consider the tsunami signal at Vi where the 410 s. peak is dominant (Fig. 11). If we apply a low-pass filter, we obtain quite a representative signal (Fig. 8) with a periodicity coherent with observations. Besides the trough leading the first crest is not anymore dominant and this also matches most observations stating that a

crest could have been first observed. We believe that this analysis complements the one proposed by Assier-Rzadkiewicz *et al.* (2000) (simultaneous slides). We complement their studies by asserting that when the two slides are taken separately, they already explain a significant (although not a total) part of the event.

### 5.3 Potential tsunamigenic submarine landslides and coastal wave impact

From the simulation, the largest SMF named CM1 might have generated a tsunami that reached the coast with wave amplitudes as large as 5 m near the Cap d'Antibes (Fig. 12). From the Fig. 12 we are able to identify several local effects that are crucial in the vulnerability of the coast to tsunamis. The different effects, related to the local bathymetry shape and the coastal confinement, prescribe the local vulnerability which, for CM1, ranges from near-zero wave amplitude aside Nice international airport (bays west of Ni and East of Vi) to estimated 5 m near the Cap d'Antibes. It is fair to say that shoaling is important but this is not the principal mechanism that controls the wave amplitude variation along the coast. The reason is that shoaling applies in the same way along the coast but the wave amplitude varies significantly, for example, the continental slope does not differ significantly offshore the Cap d'Antibes and aside the Nice airport. Moreover, the directivity of the wave (normal to the SMF long axis) should apply in the same way in both locations. Besides, other mechanical processes like non-linearity or dispersion are not supposed to be prominent for the amplification of the wave as shown for the 2004 Indian Ocean extreme tsunami event (Ioualalen *et al.* 2007a,b). Consequently such variability must be attributed to other mechanisms that can be easily identified once we superimpose the bathymetry and associated coastal shape along with the maxima of wave amplitude (Fig. 12).

The first mechanisms is focussing. In Fig. 12, we indicated in red arrows the convex-shaped bathymetry (to the coast) and with yellow arrows the concave ones, where the former shape represents focussing and the latter is for de-focussing. Through focussing the wave converges into a restricted area that concentrates the upcoming energy. This is the case at Cap d'Antibes including the bay located west of the cape and at Lerins Islands. At these locations there is a clear concave-shaped bathymetric profile: from F0 to F1 for Lerins Islands and from F1 to F2 for the Cap d'Antibes (see the bolded 100 m isobath in Fig. 12). In these areas, the wave is re-oriented through refraction (it propagates normal to the isobaths) and focuses, generating large amplitude waves. The phenomenon generally operates at capes. However this is not something systematic. It may happen that a cape does not systematically exhibit offshore convex-shaped bathymetry. This is the case for example at the Cap de Nice located immediately west of the bay of Villefranche-sur-mer (Vi) and at the cape near Menton where bathymetric profiles do not exhibit any curvature. The size of the cape also operates. As an example, the Cap Ferrat including the bay of Villefranche-sur-mer (Vi) is of restricted area (F3–F4 convex bathymetry in Fig. 12) and consequently does not generate a focussing of an extended wave. At the Cap Ferrat, the wave amplification operates but at lower scale than at the Cap d'Antibes.

To the contrary, at open bays located east and west of Ai the concave-shaped isobaths generate wave divergence that redistributes its upcoming energy into a wider area. This is the de-focussing process. As expected for open bays, the wave is significantly spread aside. It is interesting to mention that, in some circumstances, when an open bay is boarded by a convex-shaped

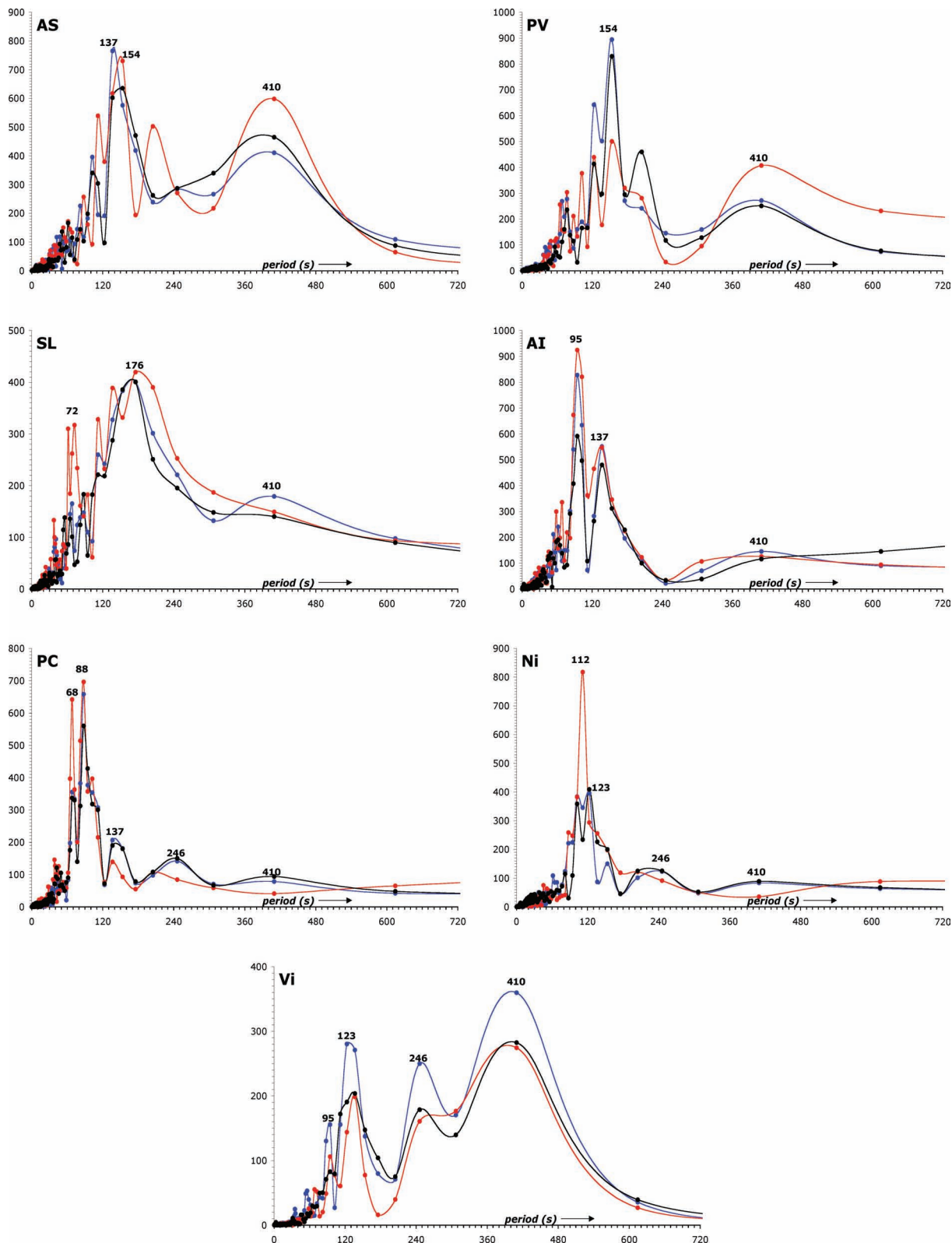


**Figure 11.** Power spectrum computed for the seven simulated time series for Vol2. Blue disks are for GEOWAVE Boussinesq fully non-linear model (BOUSS, dispersive) while red ones correspond to a non-linear shallow water model (NLSW, non-dispersive) and black ones to Linear shallow water model (LIN). Curves matching disks are for information only.

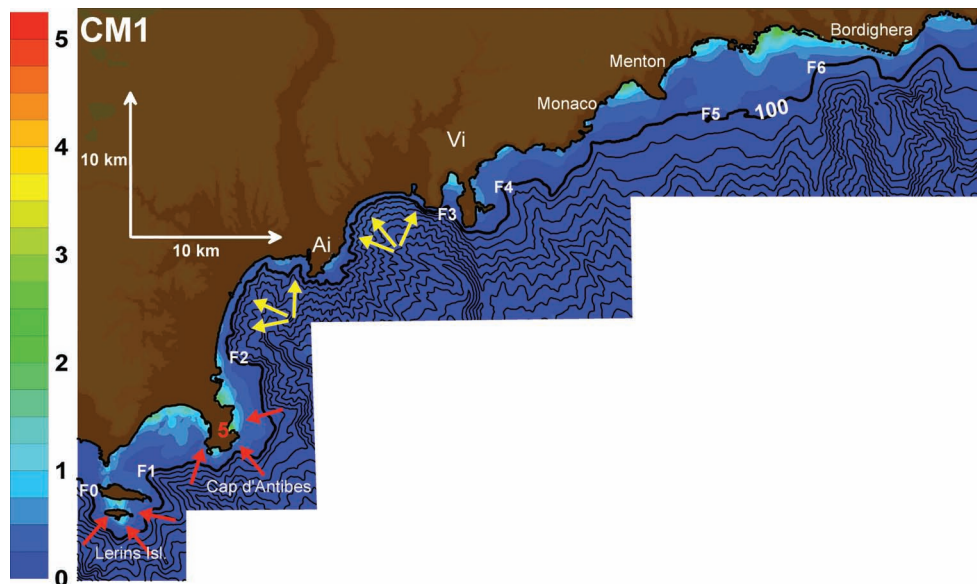


**Figure 12.** Maximum surface elevation for SMF CM1 (scale ranges from 0 to 5 m). The background bathymetry is plotted at 100 m contour intervals. Note that within our spatial grid resolution the last inundated point most of the time corresponds to the location of the maximum wave elevation. So the wave amplitudes provided in the Figure are a slight overestimate of the run up.

bathymetry, for example, the Cap d'Antibes, the wave at the open bay escapes from its sides and enhances the focussing at the cape.

The relatively high waves ranging from east of Menton to west of Bordighera (F5–F6 in Fig. 12) are difficult to explain. The bathymetric shape is trending slightly convex and may generate a weak focussing process. This possible mode of amplification may be enhanced by the presence of a relatively concave-type bathymetry immediately east of F6 that redirects the wave into the focusing area. No clear process is identified here. At Menton a trapped edge wave (west of the cape oriented SW) may possibly be responsible for the relatively high wave here. No clear evidence however.

For other SMFs (CM2, CM3 and GIProf), the statements above apply in a generic way (Fig. 13). Whatever are the sizes of the slid volumes and the associated maxima of wave steepness, we found the same robust features and the same vulnerability mapping. This is interesting because the results may apply to other regions. From SMFs CM3 to CM1 through CM2 and GIProf, the sizes of the associated tsunamis range from centimetres to meters and, however, obey to the same local mode of amplification.

The simulations show that the Ligurian coast is vulnerable to landslide-generated tsunamis that can reach significant wave amplitudes at certain locations. The largest SMF CM1 may have generated a maximum wave amplitude of order 5 m at a bay south of AS. Fig. 14 shows an estimate of the run up distribution. In the computations, the maxima of wave amplitudes are recorded at each grid point (Fig. 12) and we apply the associated local land elevation in Fig. 14. Thus we obtain an estimate (a minima) of the run up (3 m at that bay) since our grid spacing is of 100 m only. Obviously, one can expect that a more accurate simulation using a much smaller grid spacing may yield a significantly larger run up. The (minimum) run up distribution of Fig. 14 has similar features than the already discussed wave maxima. The triggering SMF was nearly at the bottom of the continental slope and the derived tsunami has been modelled with a weak slope ( $4^\circ$ ), taken as an average from the base of the slope to the basin. We may anticipate that the region

may experience much significant waves for shallower landslides triggered on the upslope, that also presents higher slope angle ( $12^\circ$ ), two wave amplifying factors.

## 6 DISCUSSION

During the past 500 yr, a dozen of tsunamis have been observed in the Ligurian Sea and most of them are associated with earthquakes with the exception of the 1979 event (Tinti *et al.* 2004). However, most of the earthquakes are weak to moderate (amplitude lower than  $M_w = 4$ ) and thus are not likely to generate recurrent significant tsunamis (Baroux *et al.* 2006). The Ligurian area experiences approximately 300 earthquakes yearly but only 3 or 4 are felt by populations. One of the most powerful earthquake of the last 1000 yr is the 1887 February 23 event (greater than  $M_w = 6$ ), that caused significant damages and casualties. However, the generated tsunami was of relatively low amplitude: tide gauges in Genoa and Nice recorded wave amplitudes of  $\sim 2$  and 20 cm respectively (versus mean sea level) and 1–2 m of typical run up were observed (Eva & Rabinovitch 1997). As far as distant tsunamis are concerned, only earthquakes generated offshore Algeria, at the junction of the Eurasian and African plates, may affect the area. However the directivity of such tsunamis is oriented northward and thus are very unlikely to affect the Ligurian basin. As an example, the  $M_w = 6.8$  earthquake that occurred the 2003 May 21, generated significant waves northward in Balears Islands but with no trace in the Ligurian sea (Delouis *et al.* 2004; Yelles *et al.* 2004; Alasset *et al.* 2006).

The 1979 October 16 Nice airport tsunami has been tentatively modelled. For that purpose we have identified two main phases in the failure evolution on the seafloor in the immediate vicinity of the airport. The initial volumes and characteristics have been reconstructed and were used to perform two single simulations. The results are discussed and compared to observations in terms of arrival times, amplitudes, crest/depression wave sequences and periodicity. Former studies performed by Assier-Rzadkiewicz *et al.*

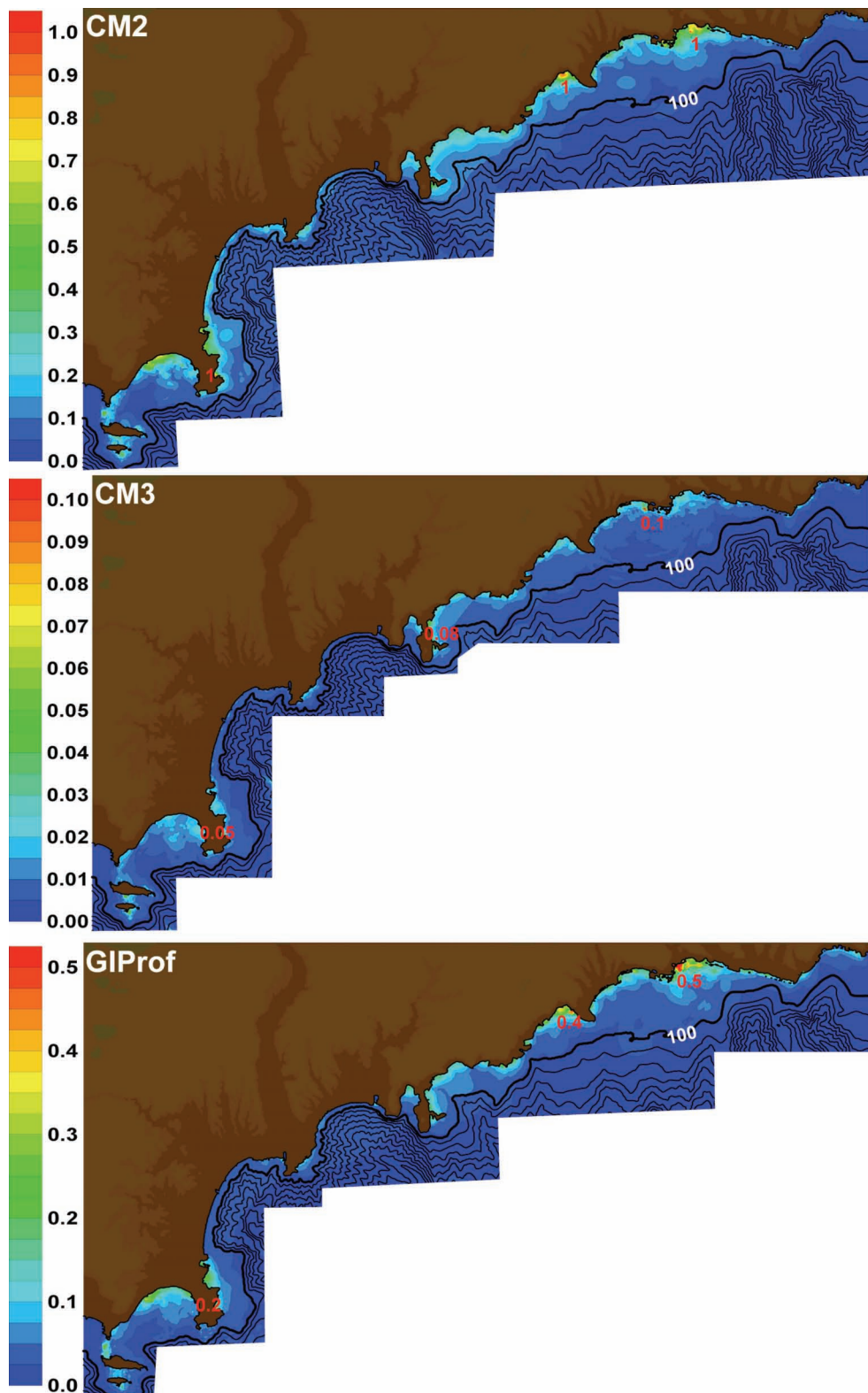


**Figure 13.** Maximum surface elevation for SMFs CM2 (scale ranges from 0 to 1 m), CM3 (scale ranges from 0 to 0.1 m) and GIPProf (scale ranges from 0 to 0.5 m). The background bathymetry is plotted at 100 m contour intervals.

(2000) showed that only simultaneous (interacting) slides could explain the event, especially to match the observed periods that are much larger than the simulated ones. As an example, Watts (1998) showed that the period of an SMF-generated tsunami depends on its

characteristic time and on the depth. If we suppose that the depth is correct in our study only an added acceleration to the deeper phase of the failure event could have increased its characteristic time. Although we have used more accurate SMF volumes and a dispersive

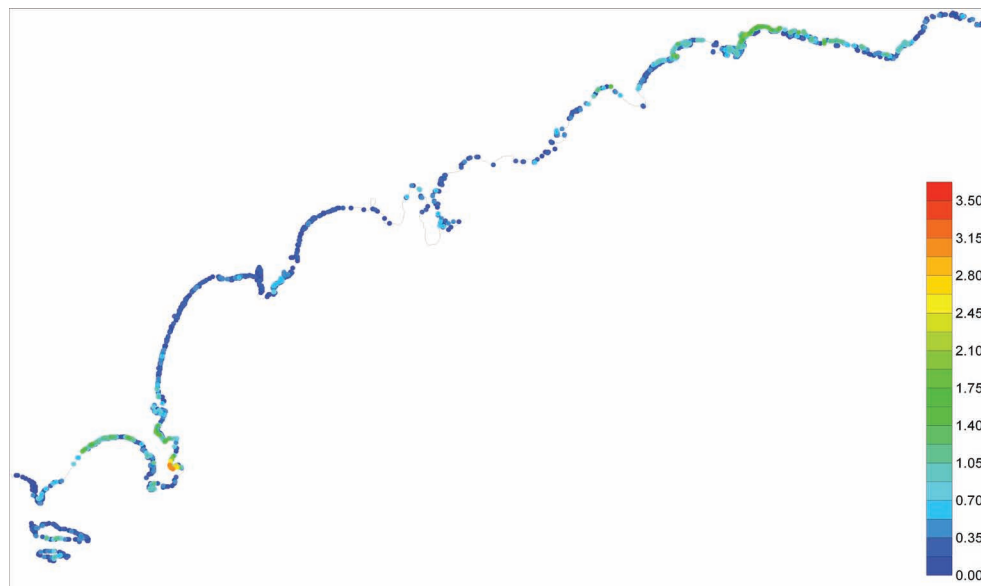


**Figure 14.** Locations of the inundated land points and their associated land height for SMF CM1. The most distant points from the coastline represent the simulated run up. This one necessarily underestimates the expected run up considering the 100 m horizontal grid spacing of our computational domain. The coastline is represented by a black line. When only the coastline is represented there is no inundation.

tsunami propagation model, we reach similar conclusions. We have analysed the effects of dispersion and found out that it is not essential for our case study. Then we have performed a basic harmonic analysis which, we believe, complements the conclusions proposed by Assier-Rzadkiewicz *et al.* (2000) (simultaneous slides). We complement their studies by asserting that when the two slides are taken separately, they already explain a significant (although not a total) part of the event.

It has been shown that older SMFs which scars are clearly observable on the present-day seafloor might have been tsunamigenic. Estimates of the maxima of amplitude of the triggered tsunami have been computed. It is fair to say that the provided absolute values have to be taken cautiously because the initial wave has not been directly computed through a reliable method. However, we would like to stress that our intention here is to provide a reasonable picture of the variability of this value along the coast and not specific maximum loads of the wave. For that purpose, we focussed our study on the identification of the local effects/mechanisms that might prescribe such variability of the vulnerability. These were the focussing/defocussing effects that depend on the convexity/concavity of the bathymetric profile and the shape of bays that may generate wave amplification through wave crest accumulation (for closed bays or bays with linear offshore bathymetry). Through different classes of SMFs (mainly characterized by different volumes), we showed that the identified features are robust because they apply for all ranges of wave steepness ranging from centimeters (CM3) to meters (CM1). They are eventually generic since they can apply in other regions.

Finally it is fair to mention that the simulated run ups indicate a real vulnerability of local areas to tsunamis. The selected older SMFs lie at relatively deep water and one may expect future shallower SMFs on the upper continental slope (Migeon *et al.* 2007). Simulations using Vol1 and Vol2 that are much shallower than CM1-3 indicate significant run ups (of same order of CM1) for much weaker involved volumes. We did not simulate here potential shallow SMFs but one may reasonably expect local run ups of order 5–10 m for volumes of order of 2 km<sup>3</sup>. We again stress that

the regions of potential strong run ups have been identified in the study.

The study of this variability is crucial to operate a tsunami warning system in the area. In the region, the continental shelf is very narrow (hundreds of meters) and the SMFs, occurring on the slope are thus very close to the coast. Typically the tsunami arrival time is of the order of a few minutes. Consequently, it is important to identify clearly vulnerable areas because with such short time scales, a warning system covering the entire area would be out of reach and especially if one considers the large occurrence time scale of SMFs. Besides, such estimates of the variability may help in optimizing an eventual instrumentation of the area. In particular few pressure gauges would be sufficient, e.g. offshore Cap d'Antibes and west of Bordighera.

## ACKNOWLEDGMENTS

The authors acknowledge with thanks the support of the Agence Nationale pour la Recherche, ANR, through the TSUMOD Grant ANR-05-CATT-016-02), the 'pole Mer' of PACA region, the GIS-CURARE and TRANSFER European project. Finally, the authors appreciated the help of the two reviewers who contributed to a substantial improvement of the first draft manuscript.

## REFERENCES

- Alasset, P.-J., Hébert, H., Maouche, S., Calbini, V. & Meghraoui, M., 2006. The tsunami induced by the 2003 Zemmouri earthquake ( $M_w = 6.9$ , Algeria): modelling and results, *Geophys. J. Int.*, **166**, 213–226.
- Assier-Rzadkiewicz, S., Heinrich, P., Sabatier, P.C., Savoye, B. & Bourillet, J.F., 2000. Numerical modeling of a landslide-generated tsunami: the 1979 Nice event, *Pure appl. Geophys.* **157**, 1707–1727.
- Baroux, E., Béthoux, N. & Bellier, O., 2006. Analyses of the stress field in the Southeastern France from earthquake focal mechanisms, *Geophys. J. Int.*, **145**, 336–248.
- Canals, M. *et al.*, 2004. Slope failure dynamics and impacts from seafloor and shallow sub-seafloor geophysical data: case studies from the COSTA Project, *Mar. Geol.*, **126**, 48–56.

- Chen, Q., Kirby, J.T., Dalrymple, R.A., Kennedy, A.B. & Chawla, A., 2000. Boussinesq modeling of wave transformation, breaking, and run-up. II: 2D, *J. Water., Port, Coastal, Ocean Eng.*, **126**, 39–47.
- Cochonat, P., Bourillet, J.-F. & Savoye, B., 1993. Geotechnical characteristics and instability of submarine slope sediments, the Nice slope (N-W Mediterranean sea), *Mar. Georesour. Geotechnol.*, **11**, 131–151.
- Dan, G., Sultan, N. & Savoye, B., 2007. Nice harbour catastrophe revisited: trigger mechanism inferred from geotechnical measurements and numerical modelling, *Mar. Geol.*, **245**, 40–64.
- Delouis, B. *et al.*, 2004. Slip distribution of the 2003 Boumerdes–Zemmouri earthquake, Algeria, from teleseismic, GPS, and coastal uplift data, *Geophys. Res. Lett.*, **31**, L18607, doi:10.1029/2004.GL020687.
- Eva, C. & Rabinovitch, A.B., 1997. The February 23, 1887 tsunami recorded on the Ligurian coast, Western Mediterranean, *Geophys. Res. Lett.*, **24**, 2211–2214.
- Fryer, G.J., Watts, P. & Pratson, L.G., 2004. Source of the great tsunami of 1 April 1946: a landslide in the upper Aleutian forearc, *Mar. Geol.*, **203**, 201–218.
- Garziglia, S., Ioualalen, M., Migeon, S., Ducassou, E., Sardoux, O., Brosolo, L. & Mascle, J., 2007. Triggering factors and tsunamigenic potential of a large submarine mass failure on the Western Nile Margin (Rosetta area, Egypt), in *Advances in Natural and Technological Hazards Research, Submarine Mass Movements and Their Consequences*, Vol. 27, pp. 347–355, eds Lykousis, V., Sakellariou, D., Locat, J., Springer, Dordrecht.
- Grilli, S.T., Ioualalen, M., Asavanant, J., Shi, F.F., Kirby, J.T. & Watts, P., 2007. Source constraints and model simulation of the December 26, 2004 Indian Ocean tsunami, *J. Water., Port, Coastal, Ocean Eng.*, **133**, 414–428.
- Grilli, S.T., Vogelmann, S. & Watts, P., 2002. Development of a 3D numerical wave tank for modeling tsunami generation by underwater landslides, *Eng. Anal. Boundary Elements*, **26**(4), 301–313.
- Habib, P., 1994. Aspects géotechniques de l'accident du nouveau port de Nice, *Revue Française de Géotechnique*, **65**, 2–15.
- Ioualalen, M., Asavanant, J., Kaewbanjak, N., Grilli, S.T., Kirby, J.T. & Watts, P., 2007a. Modeling the 26th December 2004 Indian Ocean tsunami: case study of impact in Thailand, *J. geophys. Res./Oceans*, **112**, C07024, doi:10.1029/2006.JC003850.
- Ioualalen, M., Pelinovsky, E., Asavanant, J., Lipikorn, R. & Deschamps, A., 2007b. On the weak impact of the 26 December Indian Ocean tsunami on the Bangladesh coast, *Nat. Hazards Earth Syst. Sci.*, **7**, 141–147.
- Ioualalen, M., Pelletier, B., Watts, P. & Regnier, M., 2006. Numerical modeling of the 26th November 1999 Vanuatu tsunami, *J. geophys. Res./Oceans*, **111**, C06030, doi:10.1029/2005.JC003249.
- Kennedy, A.B., Chen, Q., Kirby, J.T. & Dalrymple, R.A., 2000. Boussinesq modeling of wave transformation, breaking, and run-up. I: 1D, *J. Water., Port, Coastal, Ocean Eng.*, **126**, 39–47.
- Klaucke, I. & Cochonat, P., 1999. Analysis of past seafloor failures on the continental slope off Nice (SE France), *Geo-Mar. Lett.*, **19**, 245–253.
- Klaucke, I., Savoye, B. & Cochonat, P., 2000. Patterns and processes of sediment dispersal on the continental slope off Nice, SE France, *Mar. Geol.*, **162**, 405–422.
- Lee, H.J., Ryan, H.F., Haeussler, P.J., Kayen, R.E., Hampton, M.A., Locat, L., Suleimani, E. & Alexander, C.R., 2007. Reassessment of seismically induced tsunamigenic submarine slope failures in Port Valdez, Alaska, USA, in *Advances in Natural and Technological Hazards Research, Submarine Mass Movements and Their Consequences*, Vol. 27, pp. 357–365, eds Lykousis, V., Sakellariou, D., Locat, J., Springer, Dordrecht.
- McAdoo, B.G. & Watts, P., 2004. Tsunami hazards from submarine landslides on the Oregon continental slope, *Mar. Geol.*, **203**, 235–245.
- McMurthy, G.M., Watts, P., Fryer, G.J., Smith, J.R. & Imamura, F., 2004. Giant landslides, mega-tsunamis and paleo-sea level in the Hawaiian Islands, *Mar. Geol.*, **203**, 219–233.
- Migeon, S. *et al.*, 2007. Morphological evidences of recent submarine landslides on the Ligurian Margin (North-eastern Mediterranean): first results from Malisar cruise, in *Proceedings of the 38th CIESM Congress*, Istanbul, pp. 110.
- MIP, 1981. Mission d'Inspection Pluridisciplinaire sur le sinistre de Nice du 16 octobre 1979, Unpublished final report.
- Mulder, T., Savoye, B., Syvitsky, J.P. & Cochonat, P., 1996. Origine des courants de turbidité enregistrés à l'embouchure du Var en 1971, *C. R. Acad. Sci. Paris, série IIA*, **322**, 301–307.
- Mulder, T., Savoye, B. & Syvitsky, 1997. Numerical modelling of a mixed-sized gravity flow: the 1979 Nice turbidity current (dynamics, sediment budget and seafloor impact), *Sedimentology*, **44**, 395–326.
- Pelinovsky, E., Kharif, C., Riabov, I. & Francius, M., 2001. Study of tsunami propagation in the Ligurian sea, *Nat. Hazards Earth Syst. Sci.*, **1**, 195–201.
- Piper, D.J. & Savoye, B., 1993. Process of late quaternary turbidity current flow and deposition on the Var deep-sea fan, Northwest Mediterranean Sea, *Sedimentology*, **40**, 557–582.
- Tinti, S., Bortolucci, E. & Romagnoli, C., 1999. Modeling a possible Holocene landslide-induced tsunami at Stromboli volcano, Italy, *Phys. Chem. Earth*, **24**(5), 423–429.
- Tinti, S., Maramai, A. & Graziani, L., 2004. The new catalogue of Italian tsunamis, *Nat. Hazards*, **33**, 439–465.
- Walder, J.S., & Watts, P., 2003. Evaluating tsunami hazards from debris flows, in *Submarine Mass Movements and Their Consequences*, pp. 155–162, eds Locat, J. & Mienert, J., Kluwer Academic Publishers, Dordrecht.
- Watts, P., 1998. Wavemaker curves for tsunamis generated by underwater landslides, *J. Water., Port, Coastal, Ocean Eng.*, **124**, 127–137.
- Watts, P. & Grilli, S.T., 2003. Underwater landslide shape, motion, deformation, and tsunami generation, in *Proceedings of the 13th Offshore and Polar Engrg. Conf., ISOPE03*, Honolulu, Hawaii, **3**, 364–371.
- Watts, P., Grilli, S.T., Kirby, J.T., Fryer, G.J. & Tappin, D.R., 2003. Landslide tsunami case studies using a Boussinesq model and a fully nonlinear tsunami generation model, *Nat. Hazards Earth Syst. Sci.*, **3**(5), 391–402.
- Waythomas, C.F. & Watts, P., 2003. Numerical simulation of tsunami generation by pyroclastic flow at Aniakchak Volcano; Alaska, *Geophys. Res. Lett.*, **30**(14), 1751–1755.
- Wei, G. & Kirby, J.T., 1995. A time-dependent numerical code for extended Boussinesq equations, *J. Water., Port, Coastal, Ocean Eng.*, **121**, 251–261.
- Wei, G., Kirby, J.T., Grilli, S.T. & Subramanya, R., 1995. A fully nonlinear Boussinesq model for free surface waves. Part 1: highly nonlinear unsteady waves, *J. Fluid Mech.*, **294**, 71–92.
- Yelles, K., Lammali, K., Mahsas, A., Calais, E. & Briole, P., 2004. Co-seismic deformation of the May 21st, 2003,  $M_w = 6.8$  Boumerdes earthquake, Algeria, from GPS measurements, *Geophys. Res. Lett.*, **31**, L13610, doi:10.1029/2004.GL019884.